Journal of the Serbian Chemical Society
JSCS@tmf.bg.ac.rs • www.shd.org.rs/JSCS
*J. Serb. Chem. Soc. 91* (0)1–22 (2026)
*JSCS–13511*
*Original scientific paper*
Published 6 May 2026

# Application of Floquet theory and improvement of electron current flow control in a 1D Fe–Cu molecular chain

VIOLETA N. NIKOLIĆ[1]* and JOSE F. M. L. MARIANO[2,3]

*[1]Department of Theoretical Physics and Condensed Matter Physics (020) Vinča Institute of Nuclear Sciences, National Institute of the Republic of Serbia, University of Belgrade, P.O. Box 522, 11001 Belgrade, Serbia, [2]FCT, Campus de Gambelas, University of Algarve, Faro, 8005-139, Portugal and [3]Center of Physics and Engineering of Advanced Materials (CeFEMA), IST, University of Lisbon, Av. Roviscno Pais, Roviscno Pais, Lisbon, 1096-001, Portugal*

(Received 22 August 2025, revised 5 February, accepted 18 March 2026)

*Abstract*: In this study is investigated the application of Floquet theory to a one-dimensional (1D) Fe–Cu molecular chain under periodic driving. It was demonstrated that orbital hybridization induces resonant behavior in the low-frequency regime, highlighting the potential of this system for energy-efficient and robust device applications. For the first time, a Floquet electronic friction framework – incorporating the influence of periodic driving on electron transfer – is applied to a 1D Fe–Cu molecular chain in the presence of strong light–matter interaction (LMI). Electron transport properties are analyzed, revealing the existence of an optimal driving frequency that maximizes the electric current. Two mechanisms for enhancing charge transport in the strong LMI regime are identified: a) hybridization-induced resonances and b) photon-assisted transport processes. In this work is combined Floquet band structure analysis with open-system transport modeling in a 1D Fe–Cu motif, revealing the impact of hybridization and periodic driving, on the enhancement of electron transport *via* photon-assisted resonances – an approach that bridges quasi-energy spectra and dissipative transport in a single theoretical framework. These findings provide new insights into driven low-dimensional transition-metal systems and may support the development of Fe–Cu-based materials for electrochemical applications.

*Keywords*: hybridization; photon-assisted processes; heterogeneous catalysis.

## INTRODUCTION

Nowadays, control of the electron transport attracts attention of the scientific community. One of the aspects of this control, is the impact of the periodic driving on the electron transport, which is nowadays thoroughly investigated in literature.[1–4] Theoretical approach, often applied to study electron transport, is Floquet

* Corresponding author. E-mail: violeta@vin.bg.ac.rs
https://doi.org/10.2298/JSC250822014N

theory.[5] Floquet theory represents a mathematical framework of importance in theoretical electrochemistry, because it can facilitate current experimental electrochemical research. One of the fields of electrochemistry, in which Floquet theory is used, is heterogeneous catalysis,[6–8] where the application of Floquet theory allows deeper insight into the coupled electron-nuclear dynamics.[9] Moreover, investigation of the electron transfer under different applied bias can contribute to an improved understanding of the catalysis processes, and different, related areas of electrochemistry.[10–13] In 2024, Chen *et al*. considered application of the Floquet electronic friction model in order to get deeper insight in the molecular dynamics of near metal surfaces in the presence of periodic driving and confirmed that Floquet driving affects electron transfer.[14]

On the other hand, a class of promising, but still insufficiently investigated, materials that could be used to improve electrochemical catalysis are materials containing Fe–Cu molecular chains. A literature review has shown that exploring the unique properties of Fe and Cu interactions, presented in the catalysts containing these species, could facilitate the development of more selective and efficient catalysis, which could be used for applications, related to the sustainable energy conversion processes.[15,16] To model materials, containing Fe–Cu species, researchers applied different theoretical approaches, such as: DFT theory,[17] molecular dynamics[18] and Monte Carlo simulations,[19] *ab initio* calculations,[20] *etc*.

It is important to note that, to our knowledge, Floquet quasi-energy band structure analysis and open-system transport modeling within an electronic friction framework, has not been previously established for low-dimensional Fe–Cu systems, although their application on a given system could provide deeper insight in its properties, which is of significance for its application in electrochemistry. While Floquet theory has been widely applied to periodically driven systems, its integration with open-system transport modeling at the level of band-structure-resolved analysis remains relatively unexplored. This is also of importance from the point of view of quantum research, since, until now, bridging Floquet band structure analysis with dissipative transport modeling remains a relatively underdeveloped direction in driven quantum materials research.

Accordingly, in order to gain deeper insight into improved control of electron current in materials containing Fe–Cu molecular chains, this study investigated the possibility of improving electron transport in a 1D Fe–Cu molecular chain by applying Floquet theory. For the first time, Floquet theory was used as a theoretical approach to examine this structure. Recall that the application of Floquet theory to a 1D Fe–Cu molecular chain and a 1D Fe–Cu molecular chain results in a different Floquet band structure, due to the possible presence of asymmetry in the system, which could arise if Fe is present on the Cu substrate.

In the first part of the study, the Floquet band structure of the 1D Fe–Cu structure is illustrated, with a representation of the composition of Floquet band 3.

The influence of the orbital hybridization effect on the increase in electric current in a 1D Fe–Cu molecular chain, was considered. The effect of hybridization strength on the 1D Fe–Cu molecular chain simplified band structure, is commented, with the aim of controlling the resonance frequency shift by affecting the energy gap in the investigated hybridized 1D Fe–Cu molecular chain Floquet band structure.

On the other hand, the increase in electric current can be considered by investigating the behavior of electronic states, interacting with photon modes, during the strong LMI regime, which is discussed in more detail in the second part of the study. The dependence of electric current dependence on driving frequency for a 1D Fe–Cu molecular chain is presented, by varying the the value of the chemical potential. Deeper insight into the possibility of improving the control of electric current flow in a 1D Fe–Cu molecular chain, under driving impact, in the strong LMI regime, is of importance for the practical applications of materials containing Fe–Cu chains, in the field of electrochemistry.

## MODEL AND THEORETICAL METHODS

In this work, two complementary theoretical models are employed and combined, with the aim to investigate light-driven electron transport in a 1D Fe–Cu molecular system. Model I describes a periodically driven tight-binding Fe–Cu chain, and it is used to analyze Floquet band formation and hybridization effects. Model II describes a driven open two-level junction coupled to electronic leads and vibrational baths, and it is used to compute bias-dependent current under nonequilibrium conditions.

The first model provides insight into resonance formation in the Floquet quasi-energy spectrum, while the second translates this resonance structure into transport properties under applied bias. Below will be more described each of models, in order to get deeper insight in the postulation of the theoretical model discussed in this study.

Model I, denoting to the periodically driven tight-binding Fe–Cu chain, is relied on the static tight-binding Hamiltonian, constructed by considering a 1D periodic chain, composed of alternating Fe and Cu sites, within a single unit cell.

It is important to note that we begin calculations from a tight-binding Hamiltonian formulated in a localized orbital basis, where on-site energies describe Fe and Cu atomic orbitals and hopping terms, represent nearest-neighbor coupling and hybridization. This Hamiltonian is initially written in real space. For the periodic one-dimensional Fe–Cu chain considered in the band-structure analysis, translational symmetry allows the application of Bloch's theorem. By performing a Fourier transform to momentum space, the real-space tight-binding Hamiltonian is recast into a $k$-dependent Bloch Hamiltonian $H(k)$. The Bloch Hamiltonian is therefore not a different physical model, but rather the momentum–space representation of the same tight-binding Hamiltonian under periodic boundary conditions. This representation enables calculation of the band structure and, subsequently, its Floquet extension under time-periodic driving.

Accordingly, in the frame of Model I, the system is described within a nearest-neighbor tight-binding (TB) approximation. In momentum space, the Bloch Hamiltonian is given by Eq. (1):

$$H(k) = \begin{pmatrix} \varepsilon_{\mathrm{Fe}} & t + Ve^{-ika} \\ t + Ve^{-ika} & \varepsilon_{\mathrm{Cu}} \end{pmatrix} \tag{1}$$

where $\varepsilon_{\mathrm{Fe}}$ and $\varepsilon_{\mathrm{Cu}}$ represent on-site energies, $t$ is the hopping amplitude, $V$ represents the Fe–Cu hybridization strength, $a$ is the lattice constant and $k$ is the crystal momentum. Bonding and antibonding bands are obtained by diagonalization of given Hamiltonian. Note that, the tight--binding Hamiltonian is written with off-diagonal hopping terms as $t + Ve^{-ika}$. The specific order reflects the chosen basis and Fourier convention; equivalent forms can be obtained by alternative conventions, but here is used a uniform notation for clarity.

Since the system is subjected to an external periodic field (representing an ultrafast laser), to describe time-variations of the system, the time-dependent Hamiltonian is introduced:

$$H(k,t) = H(k) + A\theta \cos \omega t \tag{2}$$

where is $A$ – the driving amplitude, $\omega$ – the driving frequency and $\theta$ – the operator of coupling the two orbitals (taken as an inter-site coupling term).

Further, Floquet construction which will be performed, is explained below. In this study was possible to apply Floquet theory on the investigated system, since the Hamiltonian is periodic in time (H($t$ + $T$) = H($t$), where $T = 2\pi/\omega$).

The Floquet Hamiltonian is defined as:

$$H_{\mathrm{F}} = H(k,t) - i\hbar\delta_{mn} \tag{3}$$

In practice, the Hamiltonian is expanded in a truncated harmonic basis $e^{in\omega t}$, while harmonics 0, ±1 are retained. This yields a finite-dimensional block matrix representation:

$$(H_{\mathrm{F}})_{mn} = H_{m-n}(k) + n\hbar\delta_{mn} \tag{4}$$

Diagonalization of this enlarged matrix yields Floquet quasi-energies and harmonic weights. The orbital composition of selected Floquet bands is obtained from the eigenvector components. The sign convention in the last term of Eq. (4) arises from the definition of the Floquet harmonics, where the phase factor ($e^{-ika}$) corresponds to hopping from Fe to Cu sites in the chosen unit cell; this convention ensures consistency of the Hamiltonian matrix elements across all harmonics. For clarity, only the first three harmonics ($m$ = 0, ±1) are retained in the discussion (see Numerical Methods for the general truncation to $m = -N\_F,...,N\_F$, where the results are shown for $N\_F$ = 3).

Numerical procedure, performed in order to apply Model I on a considered system, was based on the construction of $H(k)$, for each value of $k$. Afterwards, it was builded truncated Floquet matrix, which diagonalization was performed numerically, and quasi-energies and orbital weights were extracted, for each vlaue of $k$. All calculations were performed, using standard matrix diagonalization routines in Matlab (R2022b).[21]

Model II was applied to describe driven two-level molecular junctions. In order to discuss electron transport under applied bias, an open quantum system, representing an effective Fe–Cu dimer, coupled to electronic reservoirs, was considered. The total Hamiltonian (in the case of this model) is:

$$H(t) = H_{\mathrm{mol}}t + H_{\mathrm{leads}} + H_{m\mathrm{ol\text{-}leads}} + H_{\mathrm{vib}} \tag{5}$$

Below are explained terms, of which is consisted the total Hamiltonian. The driven molecular Hamiltonian is represented as:

$$H_{\mathrm{mol}}(t)=\begin{pmatrix} \varepsilon_{\mathrm{Fe}} & \Delta + A\cos\omega t \\ \Delta + A\cos\omega t & \varepsilon_{\mathrm{Cu}} \end{pmatrix} \tag{6}$$

where $\Delta$ is the static inter-site coupling,and $A\cos\omega t$ represents laser-induced modulation.

Next, the leads (electronic reservoirs) are modelled as:

$$H_{\mathrm{leads}}=\sum \varepsilon_{k,\alpha} C_{k\alpha}{}^{\dagger} C_{k\alpha} \tag{7}$$

where index $k$ depicts to the quantum number for a state in the lead, index $\alpha$ depicts to the left or right lead, $\varepsilon_{k\alpha}$ is energy of the single-particle state $k$ in lead $\alpha$, $c_{k\alpha}{}^{\dagger}$ is Fermionic creation operator for an electron in state $k$ of lead $\alpha$, and $c_{k\alpha}$ – Fermionic annihilation operator for an electron in state $k$ of lead $\alpha$. These Hamiltonian models the leads as noninteracting electron reservoirs. Each lead has a continuum of states with energies $\varepsilon_{k\alpha}$. Electrons in these leads can tunnel to the molecule *via* the coupling Hamiltonian.

Considering chemical potentials, $\mu_{\mathrm{L}}$ and $\mu_{\mathrm{R}}$, the applied bias is defined as:

$$V_{\mathrm{bias}}=\mu_{\mathrm{L}}-\mu_{\mathrm{R}} \tag{8}$$

Molecule-lead coupling is illustrated as:

$$H_{\text{mol-leads}}=\sum (t_{\alpha} C_{k\alpha}{}^{\dagger} d_{\alpha} + h.c.) \tag{9}$$

where is $t_{\alpha}$ – molecule–lead hopping amplitude (coupling strength) for lead $\alpha$ (it determines impact of electrons tunneling between molecule and lead), $d_{\alpha}$ – annihilation operator for the molecular orbital connected to lead $\alpha$ ($d_{\mathrm{L}}$ couples to left, $d_{\mathrm{R}}$ to right), $c_{k\alpha}{}^{\dagger}$ – creation operator for electron in lead state $k\alpha$, and *h.c.* is Hermitian conjugate (representing addition of the term $t_{\alpha}{}^{\%*} d_{\alpha}{}^{\dagger} c_{k\alpha}$). This term allows electrons to hop between the molecule and the leads. The rate of tunneling depends on $|t_{\alpha}|^2$ and the lead density of states.

Finally, vibrational coupling is incorporated in the model, by considering nuclear vibrational modes, modelled as harmonic oscillators, coupled linearly to electronic populations:

$$H_{\mathrm{vib}}=\sum \left( \frac{p_i^2}{2M_i} + \frac{1}{2} M_i \Omega_i^2 x_i^2 \right) \tag{10}$$

where is $p_i$ – momentum operator of vibrational mode $i$, $x_i$ – position perator of vibrational mode $i$, $M_i$ – effective mass of vibrational mode $i$ and $\Omega_i$ – angular frequency of vibrational mode $i$. In other words, each molecular vibration is modeled as a harmonic oscillator. Vibrational modes can couple to electronic populations and influence tunneling rates (electron–phonon coupling).

In order to postulate Master equation, the Born, Markov, secular and wide-band approximations were applied, resulting in the reduced desity matrix, $\rho(t)$:

$$\frac{\partial \rho}{\partial t}=\frac{-i}{\hbar}\left[H_{\mathrm{mol}}(t),\rho\right]+L_{\mathrm{leads}}\left[\rho\right]+L_{\mathrm{vib}}\left[\rho\right] \tag{11}$$

where $L_{\mathrm{leads}}$ described tunneling-induced dissipation (electron tunneling under the wide-band approximation) and $L_{\mathrm{vib}}$ illustrated vibrational relaxation, with application of secular approximation, and assuming that leads are in thermal equilibrium with Fermi functions:

$$F_{\alpha}(E)=\frac{1}{1+\mathrm{e}^{(E-\mu_{\alpha})/k_{\mathrm{B}}T}} \,.$$

The master equation in the Supplementary material to this paper (Eq. (S1)) shows the same evolution in an expanded form, explicitly separating the dissipative contributions from the leads

and vibrational environment. To define current from lead $\alpha$ ($I_\alpha$, describing measure of steady--state electron flow from lead $\alpha$, into the molecule), computations are performed, based on Eq. (12):

$$I_\alpha = Tr\left[J_\alpha \rho_{ss}\right] \tag{12}$$

where $J_\alpha$ – the current superoperator (derived from the lead dissipator), associated with electron transfer through lead $\alpha$; $J_\alpha$ represents current superoperator, corresponding to electron tunneling through lead $\alpha$ (this magnitude is formally derived from $H_{\text{mol-lead}}$), $\rho_{ss}$ is steady-state density matrix of the molecule (obtained, after solving the master equation) and represents race over molecular degrees of freedom. Eq. (12) calculates the expectation value of the current in the steady state. Electrons flow from leads into the molecule (or vice versa) depending on chemical potential difference (bias). For frequency-dependent plots, the current is normalized with respect to its maximal value for fixed bias. Accordingly, Eq. (12) shows the current in normalized units ($I/I_0$), and does not include the elementary charge, $e$.

In the case of Model II, numerical procedure for its implementation in a postulated theoretical model, was as follows. First are constructed finite Hamiltonian matrices, then Floquet diagonalization is performed. Afterwards, it was considered time-evolution of master equation, and steady-state extraction, after which is performed evaluation of expectation values.

No *ab initio* or quantum-chemical electronic structure calculations were performed. All simulations rely on model Hamiltonians and standard linear algebra routines.

All parameter values used in the simulations are explicitly listed in Table I.

TABLE I. Parameters used in all numerical simulations of the 1D Fe–Cu chain, including tight--binding, hybridization, vibrational, lead coupling and external driving values. The table provides typical ranges and units for reproducibility. All values are either representative or varied systematically in the simulations, as detailed in Matlab scripts of the Supplementary material

| Parameter | Symbol | Typical value[ref.] | Description of the parameter |
|---|---|---|---|
| Fe–Cu orbital hybridization | $V$ | 0.5–3 eV[22] | Static orbital overlap between Fe and Cu |
| Hopping amplitude | $t$ | 1 eV[23] | Tight-binding nearest-neigbor hopping |
| On-site energies | $\varepsilon_{Fe}$, $\varepsilon_{Cu}$ | 0.1 eV[24] | Site energies of Fe and Cu orbitals |
| Lead tunneling | $t_L$, $t_R$ | 0.1–0.5 eV[25] | Coupling to left/right leads |
| Vibrational frequency | $\Omega_i$ | 0.1–0.5 eV[26] | Harmonic mode frequencies |
| Vibrational mass | $M_i$ | 1 amu[27] | Effective mode mass |
| Driving amplitude | $A$ | 0–3 eV[28] | Floquet driving strength |
| Driving frequency | $\omega$ | 1–3 eV[28] | Photon energy of external field |
| Temperature | $T$ | 300 K[25] | Leads thermal equilibrium |

To understand relationship between these two models (Models I and II), applied for postulation of a theoretical model considered in this study, recall that Model I provided band--structure level understanding of orbital hybridization, Floquet sideband formation and resonance conditions, while Model II captured nonequilibrium transport, bias dependence and dissipative dynamics. Accordingly, Model II may be interpreted as an effective transport reduction of the dominant hybridized Floquet states, identified in Model I.

The theoretical models described above were implemented numerically in Matlab. For the Floquet band analysis, the tight-binding Hamiltonian of the 1D Fe–Cu chain was constructed

and expanded in a truncated Floquet harmonic basis; the resulting Floquet matrix was diagonalized using standard eigenvalue routines to obtain quasi-energy spectra and harmonic weights. For the transport calculations, the Master equation for the reduced density matrix was propagated in time using standard linear algebra solvers until a steady state was reached. The current through each lead was then evaluated as the trace of the current superoperator with the steady-state density matrix. These procedures rely on numerical matrix construction, diagonalization and time evolution, and do not involve *ab initio* quantum chemistry methods. All scripts and parameter values used to generate the figures are available in the Matlab scripts, archived in Zenodo.

*Numerical methods*

All numerical calculations were performed using custom scripts implemented in Matlab. The computational procedure is consisted of two independent parts corresponding to Floquet band analysis of the periodic Fe–Cu chain, and to open-system transport calculations for the driven junction model.

Floquet band structure calculations for the periodic 1D Fe–Cu chain relied on the construction of the tight-binding Hamiltonian in momentum space, Eq. (1).

Under periodic driving with field amplitude $A$ and frequency $\omega$, the time-dependent Hamiltonian is given as Eq. (2), while the Hamiltonian is expanded in a harmonic basis, Eq. (3).

The time-periodic problem is mapped onto a static eigenvalue problem in extended Floquet space by truncating the harmonic index to $m = -N_F,\ldots,N_F$. For all figures in this work, we set $N\_F$ to 3, corresponding to the retention of harmonics 0, ±1. Convergence with respect to $N_F$ was verified numerically.

The resulting block matrix is diagonalized using Matlab's standard dense eigenvalue solver (eig) to obtain quasi-energy spectra and Floquet eigenstates. Band structures are generated by sweeping $k$ across the first Brillouin zone.

Master equation transport calculations are relied on the total Hamiltonian, postulated for the driven molecular junction:

$$H(t) = H_{mol} + H_{leads} + H_{mol-leads} + H_{vib} + H_{drive}(t) \tag{13}$$

The reduced density matrix $\rho(t)$ evolves according to the Born–Markov master equation, Eq. (11). The density matrix is propagated in time using Matlab's ODE solvers, until a steady state $\rho_{ss}$ is reached.

Further, the current from lead is computed, by Eq. (12). Bias voltage is introduced *via*:

$$\mu_L = \frac{+eV_{bias}}{2}, \mu_R = \frac{-eV_{bias}}{2} \tag{14}$$

Current–bias and current–frequency characteristics are obtained by parameter sweeps over bias voltage ($V_{bias}$), driving amplitude ($A$) and driving frequency ($\omega$). The bias voltage is introduced *via* eq. (14), which enters the system Hamiltonian and thereby determines the terms appearing in eq. (8). Current–bias and current–frequency characteristics are obtained by parameter sweeps over $V_{bias}$, driving amplitude $A$ and driving frequency $\omega$.

Below are given numerical implementation details.

The numerical procedure is consisted of construction of finite-dimensional Hamiltonian matrices, Floquet matrix assembly with harmonic truncation, matrix diagonalization for quasi-energy spectra, construction of Liouvillian superoperators, time propagation of the density matrix and trace evaluation for steady-state current.

All calculations are relied on standard numerical linear algebra operations (matrix construction, diagonalization, ODE integration). No density functional theory (DFT), Hartree–Fock or correlated *ab initio* electronic-structure methods were employed. Parameter values used in all simulations are listed in Table I. All scripts used to generate the figures are available in a repository provided for peer review.

## RESULTS AND DISCUSSION

### *Impact of the orbital hybridization effect, on the electric flow in 1D Fe–Cu molecular chain*

To perform visualization of the Floquet band structure of the 1D Fe–Cu molecular chain, a corresponding simplified theoretical model was postulated. The model is relied on the tight-binding (TB) model,[29] which has been applied to describe the irradiation of a Fe–Cu unit cell, by an ultrafast intense laser. The postulated model described the interaction between light and the Fe–Cu chain, resulting in the appearance of photons. The represented visual illustration enabled further mathematical tracking of the impact of the produced photon on the original band. In this manner, a deeper insight into the electronic landscape of the Fe–Cu molecular chain is provided, in which the second part of the study will provide a mathematical description of the electron transfer (modeled *via* electron tunneling), occurred through the chain.

Let us recall that the TB model is often applied to describe the electronic structure of a given material. In the case of our model, relied on the TB model, a uniform 1D molecular chain was considered, in which electrons are localized, but could tunnel between neighboring chemical species in the considered molecular chain. In order to prepare the appropriate Matlab code, it was necessary to propose an appropriate Hamiltonian to describe a uniform 1D molecular chain. The proposed simplified Hamiltonian consisted of two terms: the first term describes the energy of the localized electron (*i.e.*, the on-site energy) and the second term represents a hopping term, which describes the amplitude of the probability of the electron tunneling to a neighboring site. Consideration of Bloch's theorem enabled the preparation of Matlab code for solving the eigenvalue problem[30] in order to obtain two energy bonds. In the visual illustration, these bonds are represented as bonding and antibonding bonds, represented by the same color (Fig. 1a). Further, the Matlab code is modified in order to illustrate the application of Floquet theory to our considered case, *i.e.*, to a periodically driven 1D Fe–Cu-like chain. The code was written by considering the periodical drive of the given system (the driving of the system induces a time dependence of the tight-binding Hamiltonian), and the quasi-energy spectrum was obtained by diagonalizing the enlarged Floquet Hamiltonian. As a result of applying the simplified Floquet theory to the case of a periodically driven 1D Fe–Cu molecular chain, Fig. 1b and c were obtained.

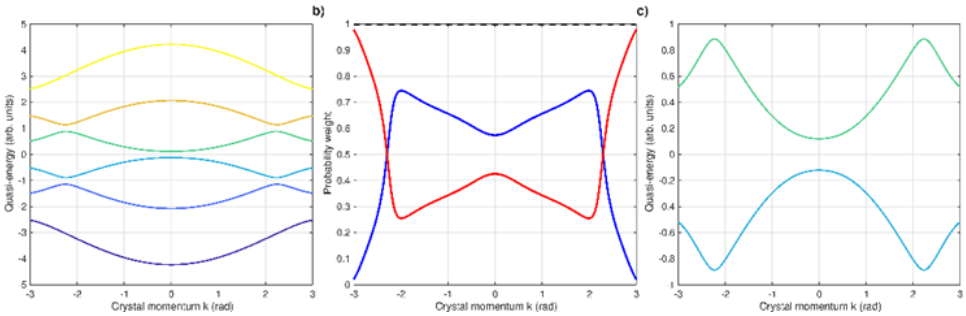


Fig. 1. Floquet band structure and orbital composition of a periodically driven 1D Fe–Cu molecular chain under strong driving ($t_1 = 0.6$, $\omega = 2$): a) Floquet quasi-energy band structure of the periodically driven 1D Fe–Cu chain, obtained from the $k$-dependent Bloch Hamiltonian under harmonic driving (the colors of the curves are used for visual clarity to distinguish different bands and do not correspond to a particular orbital, atom, or photon contribution); b) harmonic composition (Floquet mode weights) of the third quasi-energy band, illustrating the mixing of photon sectors induced by periodic driving (blue curve corresponded to Fe orbital weight, red curve to Cu orbital weight, and black dashed curve to the photon component); c) full quasi-energy spectrum showing the formation of Floquet replicas and hybridization-induced gap modification.

To understand Fig. 1, let us recall that the Floquet state represents a solution to the time-dependent Schrödinger equation, based on the considered Hamiltonian. In Fig. 1, Floquet states are represented as superpositions of harmonics, characterized by a resonance driving frequency. As a result, a photon appears in the system, the energy of which is specifically equal to the gap between the bonding and antibonding orbitals appears in the system. In other words, the resonance condition for the interaction between an external periodic field (laser), characterized by frequency $\omega$, and the energy gap between the ground and excited state (bonding and antibonding state, respectively) of the system under consideration is estimated as: $\hbar\omega \approx \Delta E$, where $\hbar\omega$ represents photon replica bands. The driving of molecule in resonance results in the fact that a single Floquet state can be characterized by both, bonding and antibonding features. Consequently, this could lead to a new Floquet eigenstate, characterized by hybrid, mixed properties of both, the bonding and antibonding states.

Fig. 1a represents the evolution of averaged (quasi) bands, in a system with a 1D molecular chain, consisting of two sublattices (Fe and Cu), as a function of the crystal momentum $k$, in the presence of a time-periodic drive. It provides visualization of band hybridization, occurred due to interaction with a photon, in the vicinity of resonance. Since Fe and Cu are characterized by d-band structures and different electronegativities, the corresponding on-site energies differed significantly for these two atoms.

In a weak driving regime, Fig. 1a would provide a visualization of three harmonics (*i.e.*, the original band, the band shifted up by $+\hbar\omega$, and the band shifted

down by $-\hbar\omega$), composed of two orbitals (resulting in 6 lines). In the case of weak driving, observed three harmonics could be interpreted as three bands: the original band (characterized by the absence of shift), harmonic (band) shifted downward, and harmonic shifted upward. Since in a given case, it was considered strong driving of the investigated system, each colored line represented a distinct quasi-energy band, where is color of the line used for visual clarity. Under strong periodic driving, the quasi-energy bands arose from significant hybridization between different Floquet photon sectors, and each quasi-energy band becomes a mixture of many harmonics, so it is not possible to ascribe one color of the curve to the certain harmonic.

Fig. 1b represents a visualization of the orbital composition (probability weights of Fe and Cu orbitals) of a chosen Floquet band (in our case, Floquet band 3 was chosen), dependent on the crystal momentum, $k$. It represents the Floquet band composition across the Brillouin zone, describing electron tunneling between Fe and Cu species, along a 1D chain. Since the momentum $k$ provides an information about the electron wavelength and the phase relations between orbitals, the orbital composition shows a complex dependence on $k$, characterized by hybridization effects.

Fe and Cu contributions illustrate the impact of the Floquet state on the mixing of the electronic and photonic character along the chain. The band eigenstate probability weights describe the extent to which the eigenstate at Floquet band 3 (for a given momentum, $k$) is localized on Fe or Cu orbitals (or mixed hybridization is represented). The total photon weight (illustrated by the black dashed curve, which represents the weight of Fe + the weight of Cu, summed over all Floquet harmonics) represents the photon composition. The blue line depicts to the total Fe orbital weight summed over all Floquet harmonics for band 3, for each value of $k$ (and the red line shows the Cu orbital weight, respectively). The high Fe or Cu weight (at a given $k$), confirms that the electron, in a given Floquet state, shows an affinity to behave as a localized d-atom of Fe (or Cu, respectively). It should be noted that Floquet band 3 illustrates a mixed Fe–Cu character, depicting to the dominance of Fe or Cu orbitals (characteristic for given electronic states), at different moments. Strong LMI hybridization is confirmed by the fact that the photonic component shows relatively uniform behavior, while representing a significant part of the Fig. 1b.

It is worth noting that Floquet band 3 corresponds to a particular Floquet quasi-energy band that evolves from one of the hybridized bands.[31]

The composition of Floquet band 3 (Fe, Cu, and photon weights) reflects the extent to which the original Fe and Cu orbitals experienced hybridization, combined with the photon interaction induced by the drive. As a result of the hybrid nature of Floquet band 3, this band plays the most important role in light-induced transport, as electrons are characterized by the ability to absorb or emit photons,

which could be reflected in the spectrum, as a shift in energy and momentum. It is known that the Floquet band structure of a periodically driven 1D Fe–Cu molecular chain is significantly affected by the impact of strong LMI. As a result of the LMI impact, electron–photon quasi-particles are formed.[32] Consequently, the Floquet bands are strongly affected, as new gaps open at the photon resonances, leading to the appearance of new Floquet sidebands. In other words, the strong LMI regime induces a large photonic component in Floquet band 3, observed in Fig. 1b, which ensures band hybridization, which, further, results in high sensitivity to changes in the driving frequency of the investigated system (1D Fe–Cu molecular chain).

Fig. 1c shows the dependence of the Floquet quasi-energy bands on the crystal momentum $k$, which is discussed for Floquet band 3. It is shown chosen colored curves, corresponding to a quasi-energy band, with colors again used only to distinguish bands visually.

Fig. 1 is given with the aim of enabling visualization of the electronic structure of the 1D Fe–Cu chain, as it represents theoretical material used for mathematical monitoring of electron tunneling, described in more detail in the rest of the paper. It illustrated different aspects of the driven 1D Fe–Cu system: Fig. 1a shows the simplified band structure, Fig. 1b highlights the orbital/photon composition of a selected band and Fig. 1c presents the chosen Floquet spectrum.

After introducing the electronic structure of the 1D Fe–Cu chain, a theoretical model is proposed, enabling a discussion of the behavior of the current under the influence of the driving. The same tight-binding model is applied, with a modification of the Hamiltonian form. The influence of photon-assisted processes is also considered.

Appropriate Matlab code was written to illustrate the electric current oscillations with the driving frequency, Fig. 2a. The current behavior is assumed to be governed by resonant photon-assisted transitions, associated with the simplified Floquet band structure of the 1D Fe–Cu chain. It should be noted that the given model was postulated to examine the dependence of current oscillations on the driving frequency, without considering the hybridization effect, or the influence of chemical potential. Fig. 2 is intended to illustrate a simple representation of the probability of photon-assisted tunneling as a function of the driving frequency $\omega$, in the form of the dependence of the normalized current on the driving frequency. In other words, it describes the effect of orbital hybridization on photon-assited tunneling and resonant transport in periodically driven molecular chains.

As expected, the current decreases rapidly with the driving frequency, indicating the absence of resonance condition. The maximum current value corresponds to optimal photon-assisted transport, when efficient absorption or emission of photons and transition between bands, occurs. The absence of resonance results in weaker photon-assisted transport. To illustrate the oscillations of the electric

current in its dependence on the driving frequency, caused by photon-assisted resonant transitions, with respect to the simplified Floquet band 3 composition, the model was modified to include the effect of orbital hybridization between Fe and Cu orbitals in Floquet band 3, and to consider its influence on the current behavior. The hybridization effect was investigated, because it is often observed in transition metal chains, such as Fe–Cu, where Fe 3d and Cu 3d orbitals interact. The corresponding model, as a premise, considered modifying the model Hamiltonian by introducing an additional hybridization term, $V$, characterizing mixing of Fe and Cu orbitals, resulting in two new hybridized bands (bonding and antibonding).

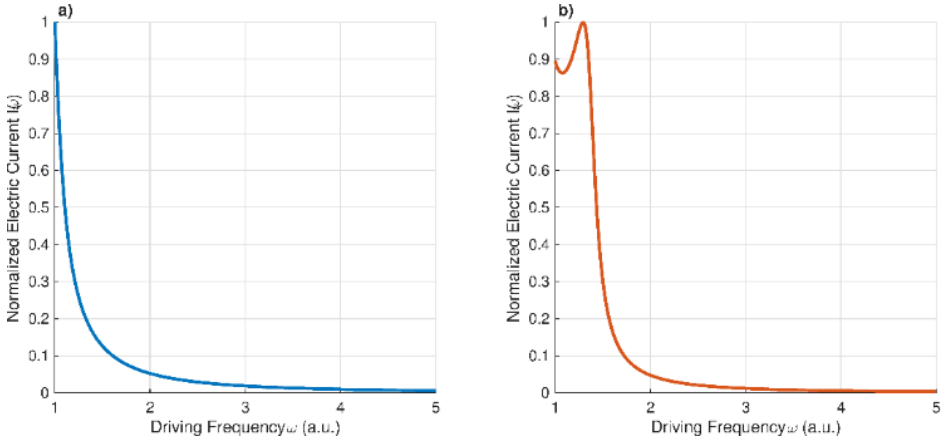


Fig. 2. Dependence of normalized current on driving frequency: a) normalized steady-state electric current as a function of driving frequency $\omega$ for the 1D Fe–Cu molecular chain in the absence of orbital hybridization ($V = 0$), showing no pronounced resonant enhancement; b) normalized steady-state current as a function of driving frequency in the presence of Fe–Cu orbital hybridization ($V \neq 0$), demonstrating resonance enhancement associated with hybridization-controlled quasi-energy gap formation.

The strength of the $V$ is defined by the distance and chemical bonding between the Fe and Cu atoms, and this quantity affects the size of the band gap. Consequently, the two hybridized bands (appeared as a result of the Hamiltonian modification), are associated with the Floquet band structure of the investigated 1D Fe––Cu molecular chain. Let us recall that the Floquet band 3 is a band which is evolved from one of these hybridized bands under strong LMI. The proposed hybridization impacts the LMI strength, which increases the current. The discussed hybridization enables the opening of gaps, allowing for enhanced photon-assisted transitions, which defines the resonant frequencies where current amplification occurs. As a result, the total current is increased and an additional resonance peak appears, as illustrated in Fig. 2b.

The observed current peak corresponds to the resonant driving frequency $\omega$, which corresponds to the energy difference between electronic states in Floquet

band 3. In other words, the system efficiently absorbs/emits photons at those frequencies, enabling electrons to more easily tunnel through the system and *vice versa*. Consequently, the current is increased or suppressed, and roughly follows the dependence observed in Fig. 2a. Fig. 2 illustrates the interplay between the Floquet band 3 composition of the 1D Fe–Cu molecular chain and a strong LMI, resulting in a highly frequency-dependent transport response. The maximum, corresponding to the driving frequency, is in resonance with the Floquet quasi-energy, enabling photon-assisted tunneling and enhanced current.

It should be noted that the observed peak, which reflects the resonant coupling between the drive and electronic transitions in the hybridized 1D Fe–Cu molecular chain, appears in the low driving frequency range, near to ~1.1 a.u., which is the low-frequency part of the spectrum. Recall that the presence of optimal photon-assisted transport at low frequencies (in the frequency range, covering the THz-mid IR) is a favorable characteristic of materials used to construct energy-efficient devices with robust operation. This is of practical importance for the application of materials, containing Fe–Cu molecular chains. Bearing in mind that new hybridized bands could only appear under the influence of an ultrafast laser (visible light cannot induce the hybridization effect and the opening of a new gap), the observed peak in the low-frequency region of the spectrum (Fig. 2b), confirms the potential usage of the investigated theoretical system of a 1D Fe–Cu molecular chain. Consequently, our modeled system could be employed for practical application in the design of devices operating at frequencies where photon-assisted transport can be efficiently tuned by hybridization effects, such as: THz detectors and sensors,[33] in infrared photodetectors[34] or in low-power optoelectronic switches and modulators,[35] quantum cascade lasers and amplifiers,[36] spintronic devices and magnetic sensors[37] and photovoltaics.[38]

On the other hand, applications of Fe–Cu molecular chains in the low frequency range could face certain disadvantages, such as lower photon energies (which limits access to higher-energy electronic transitions) or slower modulation (the lower frequency limits the velocity, which could be used for switching or modulating devices). Consequently, it could appear a need to shift the resonant peak of the Fe–Cu molecular chain towards a higher frequency range (visible light to UV). This could switch the potential use and practical application of the theoretically considered system, investigated in this study, into the field of ultrafast devices or into the field of nanoscale control. Although the adoption and modification of the considered theoretical system for the application of higher frequency resonance may require more complex materials and control, this represents a research problem that has not yet been satisfactorily resolved. Variation of a discussed parameter, the hybridization strength, in order to shift the resonant peak towards a higher frequencies, is more discussed in the Supplementary material (Fig. S-1).

*Impact of the photon-assisted processes on the electric flow in 1D Fe–Cu molecular chain*

In the second part of the study, a modified theoretical model, discussed in in the literature,[14] was applied to perform a more precise modeling of electron transfer in a 1D Fe–Cu molecular chain under driving impact, in the strong LMI regime. This approach, at the same time, enables deeper insight into the dependence of the oscillatory electric current on the driving frequency, taking into account the influence of the chemical potential. To investigate electron tunneling, within the Floquet electronic friction model, a more complex form of the Hamiltonian was considered, applied to the case of a 1D Fe–Cu molecular chain. Chen *et al*. considered a general Hamiltonian, consisting of different contributions, describing: the molecule contribution, the leads, the interaction between them, LMI (considered semi-classically) and nuclear degrees of freedom (DoF), in order to postulate a model to describe the quantum transport of a molecular junction.[14] Basically, the model Hamiltonian described a two-level molecular junction, coupled with two baths (leads), where the light induced coupling between the levels.

In our study, similar premises of the model were applied: the model considered a driven two-level system, with nuclear coordinates (bath) coupled to leads and periodic light, applied to a 1D Fe–Cu molecular chain. The given system includes a dissipative bath, in order to represent nuclear relaxation and electronic vibrational modes. The proposal of two metals Fe and Cu leads (electron baths), each with different chemical potentials, allows for the electron injection and extraction of electrons. To postulate our model, two electrons, positioned on two adjacent d-aluminum Fe and Cu orbitals, in a 1D molecular chain, were considered. The modeled system is based on several premises. First, a two-level model is proposed for the molecular part (although, to simplify the complex research issue, only the Fe site will be considered), where electron tunnel *via* coupling with Fe and Cu molecular orbitals is localized at the respective sites. The nuclear degree of freedom is then calculated, considering two vibrational modes, coupled to local Fe or Cu nuclei (as nuclear coordinates, affecting the energy level and coupling, including electronic-photon phonon coupling). Further, LMI was applied, taking into account that the investigated system is driven by an externally applied, ultrafast intense laser, periodically modulating the electronic coupling. The leads are considered in terms of the baths.[14] Finally, the postulated Hamiltonian describes the Fe–Cu molecular sites electronic tunneling, the nuclear vibrational DoF, the coupling to leads and the laser driving LMI. Light induced driving enables transitions between Fe and Cu orbitals, modulated by the term $A\cos \omega t$.[14] Accordingly, the given theoretical model describes the coupling between the Fe and Cu electron sites in a 1D Fe–Cu molecular chain, while the steady-state current is calculated as defined in Eq. (5), and its dependence on applied bias is illustrated in Fig. S-2 of the Supplementary material.

To represent the relationship between electron current and driving frequency in the strong LMI regime: $A = 5$, a corresponding Matlab code was prepared, Fig. 3. It should be mentioned that the applied bias convention (related to the chemical potentials of the leads) took into account: $\mu_L > 0$ and $\mu_R = 0$, as this enabled simplification of the preparation of the transport simulation. Consequently, bias = $\mu_L - \mu_R = \mu_L$, and the chemical potential of the left lead's is shifted positively, since the right lead is taken as a reference to zero chemical potential.

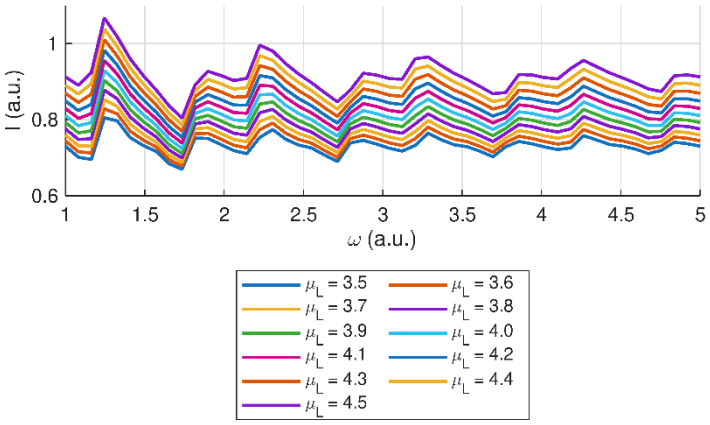


Fig. 3. Steady-state electron current as a function of driving frequency $\omega$ in the strong light–matter interaction regime ($A = 5$). The chemical potential $\mu_L$ was varied in the range 3.5–4.4 (in model energy units), while $\mu_R$ was fixed, illustrating bias-dependent resonance shifts and nonlinear photon-assisted transport behavior.

Fig. 3 illustrates the behavior of the electric current *versus* driving frequency, for different chemical potentials ($\mu_L$), ranging from 3.5 to 4.5, in arbitrary units. Multiple peaks can be observed in $I(\omega)$ for all values of $\mu_L$. It provides deeper insight into the dynamics of electric current behavior in the strong LMI regime. Regular dynamical variations in current behavior could be noticed, *i.e.*, the current decreases with the driving frequency over the entire range of applied bias. Albeit, the current periodically reaches a maximal value, while the observed maxima decrease, with increasing bias. The observed behavior confirmed Chen *et al*. conclusion about non-monotonic behavior of this dependence, and the existence of an optimal frequency that maximizes the electronic current.[14] It should be noted that Fig. 3 shows that the current oscillations behave correlated with the driving frequency, meaning that the chosen driving frequencies result in increased current.

Based on Fig. 3, the current increases, as $\mu_L$ approaches a value of 4, while decreasing thereafter. The transition from low to high current occurs smoothly, indicating that the system undergoes resonant-like amplification near $\mu_L = 4$ (in other words, the resonance condition is fulfilled at this value). The purple curve in Fig. 3 represents the highest current, which corresponds to $\mu_L \approx 4$.

The occurrence of current amplification can be understood as the result of the alignment between the driving field, at a given bias ($\mu_L = 4$), and the energy levels. One reason for recognizing the intermediate bias ($\mu_L = 4$), as the one that results in the highest current can be found in the fact that applying low biases can lead to current suppression, while very high biases can lead to saturation or dephasing effects, which can reduce the current. The intermediate bias provides the conditions which results in constructive interference or optimal occupancy probability, producing a stronger maximum. Considering the fact that the bias window characterizes the available states for electron transfer, the intermediate bias could enable a larger effective energy window, and favorable differences in occupancy between the leads, resulting in increased current.

Recall that in quantum transport, which impacts the current behavior, the bias window refers to the energy range over which electrons can flow from one lead to another, due to an applied voltage. Consequently, this is the range in which electronic states can contribute to the flow of current. It represents an optimal bias window, with the optimal number of energy levels represented within the window, so that electrons can tunnel efficiently, and resonant effects can maximize current.

Further, to find the optimal driving frequency ($\omega$) for $\mu_L = 4$, which enables the current maximum, a modified Matlab code was prepared, and the results are presented in Fig. 4a.

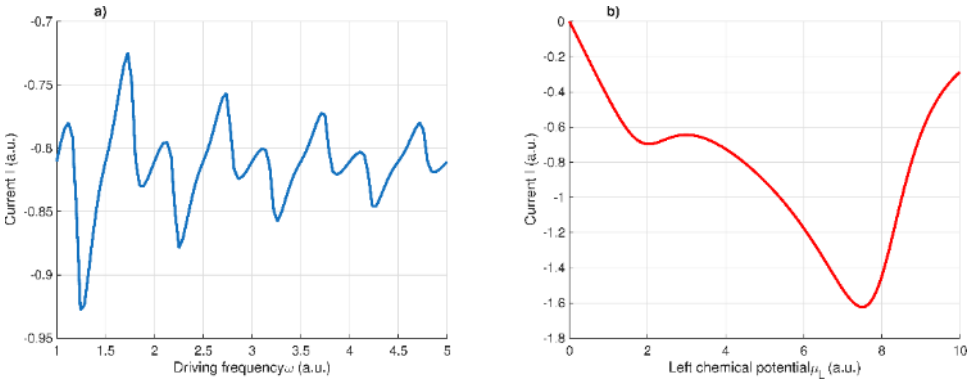


Fig. 4. Dependence of current on driving frequency: a) steady-state current as a function of driving frequency $\omega$ at fixed bias ($\mu_L = 4$, $\mu_R$ defined by the applied bias), demonstrating frequency-dependent photon-assisted transport; b) current–bias characteristics showing the dependence of steady-state current on the chemical potential $\mu_L$ (corresponding to the applied bias voltage), highlighting the modulation of transport by periodic driving. According to Fig. 4a, the current maximum is observed at $\omega$ around 1.727 a.u., which depicts to a particular driving frequency for the bias value $\mu_L = 4$. Fig. 4a) also confirms the oscillatory behavior of the given dependence, indicating a non-monotonic behavior with respect to frequency, due to the driving dynamics. Consequently, nonlinear transport dynamic under strong driving in the LMI regime was confirmed.

Fig. 4b represents the changes in current with bias at the optimal frequency; it shows the dependence of the current, on the bias $\mu_L$. In Fig. 4b, the ved current reversal illustrates the dependence of current on bias obser voltage, under resonance driving. It is observed that the current does not increase or decrease uniformly with $\mu_L$, although a drop is observed around $\mu_L$ of 7.5, followed by an increase in current. Such behavior indicates that the system is subjected to resonance-like current suppression at certain biases, even though the drive frequency is resonant. The observed drop can be explained differently: it could occur due to the presence of destructive interference between different Floquet transport channels,[39] as a result of detuning the electronic population from the driving-induced resonance condition at high $\mu_L$,[40] or due to minimized net population imbalance or suppression of the contribution of inelastic currents at a given $\mu_L$. It should be noted that at lower biases, the increase in $\mu_L$, initially, leads to an increase in current. But, after that, the current achieves plateau and decreases, indicating a nonlinear bias response and confirming the fact that strong LMI induces nonlinear effects in the system.

Noteworthy, observed feature illustrates the fact that a strong LMI would have a more significant impact on the current, once resonance is reached. The aforementioned effect could be achieved by coherent photon-assisted tunneling which induces enhancement or suppress of the current. Current oscillations appear as a result of resonant coupling between electronic transitions and the drive. The oscillator-dependence of current, observed in Fig. 4, appears as a result of the presence of frequency-dependent resonances in the electric current. If the driving value is equal to the energy difference between the states in Floquet band 3 and the other bands (which occurs at certain frequencies), enhanced photon-assisted tunneling occurs, which increases the current.

It is important to note that given 1D Fe–Cu chain model represents a theoretical model, which captures key features of bimetallic Fe–Cu motifs that are widely studied in heterogeneous catalysis and electrocatalysis, such as $CO_2$ reduction and selective hydrogenation reactions. In real systems, electron transfer between Fe and Cu sites plays a critical role in catalytic efficiency, and proposed model provides a platform to explore the impact of hybridization strength and periodic driving influence on the electron flow. The Floquet analysis simulates external periodic perturbations, which can be interpreted as light-induced or voltage-modulated excitations in experimental setups. Obtained results indicated that tuning orbital hybridization and applying controlled periodic driving can enhance resonant electron transport between active sites, offering qualitative insight into photon-assisted or dynamically modulated charge transfer in bimetallic catalysts. It should be noted that this study does not aim to quantitatively reproduce any specific Fe–Cu material or electrochemical interface, but to provide a framework

that can guide experimental strategies for improving catalytic and electrochemical performance through controlled electronic dynamics.

*Limitations of the model*

The present study is based on a minimal theoretical model designed to discuss the essential mechanisms of hybridization-controlled Floquet transport in Fe–Cu motifs. While this approach enabled analytical clarity and transparent numerical implementation, several limitations should be mentioned.

The investigated Fe–Cu system is modeled as an idealized one-dimensional periodic chain (for band analysis) and as a two-level molecular junction (for transport calculations). Real Fe–Cu catalytic materials and electrochemical interfaces possess three-dimensional geometries, structural disorder, surface reconstructions, and complex coordination environments. These structural features are not explicitly included in the present model.

In order to simplify model, electron–electron interactions are neglected beyond effective single-particle descriptions. The Hamiltonian does not include explicit Coulomb interaction terms (*e.g.*, Hubbard U), correlation effects or many-body self-energies. As a consequence, correlation-driven phenomena (such as Kondo physics, strong localization or correlation-induced gap renormalization) are not considered.

The construction of Floquet Hamiltonian is performed, using a finite truncation of photon harmonics. While convergence with respect to the number of harmonics was verified numerically for the parameter regimes considered, extremely strong driving or very high frequencies may require additional harmonics for quantitative accuracy.

Also, it could be noted that the open-system transport treatment is relied on the Born–Markov and secular approximations, characterized by assuming weak molecule–lead coupling, negligible memory effects and well-separated energy scales. In regimes of strong system–bath coupling or highly non-Markovian dynamics, the Master equation approach may lose quantitative accuracy. On the other hand, simplification of the model required to neglect the anharmonic effects, mode–mode coupling and nonequilibrium phonon populations, in order to describe vibrational modes within a harmonic approximation and their treatment as independent baths.

Further, the wide-band approximation is employed for the metallic leads, assuming energy-independent density of states near the Fermi level. Real Fe and Cu electrodes are characterized by structured densities of states, which could modify tunneling rates and resonance conditions.

Finally, the model does not aim to provide a quantitative first-principles description of a specific Fe–Cu catalytic material. Instead, it serves as a minimal

theoretical platform to explore qualitative mechanisms of hybridization-controlled resonance tuning and photon-assisted transport in Fe–Cu motifs.

Despite these limitations, the model captures the essential interplay between orbital hybridization, periodic driving and open-system transport. The simplified framework allows clear identification of resonance shifts and current enhancement mechanisms, which may guide more elaborate future studies based on DFT or experimentally characterized Fe–Cu systems.

## CONCLUSIONS

In this study is presented a detailed theoretical framework for the transport properties of a Fe–Cu molecular chain under periodic driving. Application of Floquet theory allowed modulation of electronic states *via* photon-assisted processes. Master equation approach captured electron tunneling under bias and vibrational interactions. Consequently, it is shown that hybridization control shifts the static and quasi-energy gaps, tuning resonance frequencies. Performed study demonstrated that integrating Floquet quasi-energy analysis with master-equation-based transport allows controlled modulation of electron flow in Fe–Cu chains, providing a novel perspective on driven electron dynamics that goes beyond traditional approaches focused solely on band structure or open-system transport. Futrher, the distinction between orbital hybridization (static Fe–Cu overlap) and Floquet mixing (laser-induced coupling to photon states) is clarified. The model demonstrated that careful tuning of driving amplitude and frequency can enhance or suppress electron current, providing insight for future nanoscale devices. Although idealized, presented results establish a foundational understanding of photon-assisted transport in Fe–Cu chains, forming a basis for further work connecting 1D theoretical models with realistic Fe–Cu catalytic systems or experimental electrochemical interfaces.

## SUPPLEMENTARY MATERIAL

Additional data and information are available electronically at the pages of journal website: https://www.shd-pub.org.rs/index.php/JSCS/article/view/13511, or from the corresponding author on request. The computational codes used in this study are openly available at GitHub, archived in Zenodo.[41] The repository includes scripts for constructing the $k$-dependent Bloch Hamiltonian, generating the Floquet matrix under periodic driving, performing numerical diagonalization, and reproducing the quasi-energy spectra and harmonic composition figures reported in this work.

*Acknowledgement.* The research was funded by the Ministry of Education, Science and Technological Development of the Republic of Serbia (451-03-136/2025-03/ 200017).

И З В О Д

## ПРИМЕНА ФЛОКЕОВЕ ТЕОРИЈЕ И УНАПРЕЂЕЊЕ КОНТРОЛЕ ТОКА ЕЛЕКТРОНСКЕ СТРУЈЕ У 1D Fe–Cu МОЛЕКУЛСКОМ ЛАНЦУ

ВИОЛЕТА Н. НИКОЛИЋ[1] и JOSE F. M. L. MARIANO[2,3]

*[1]Лабораторија за теоријску физику и физику кондензоване материје (020) Институт Нуклеарних Наука "Винча", Институт од националног значаја, Универзитет у Београду, п.пр. 522, 11001 Београд, [2]FCT, Campus de Gambelas, University of Algarve, Faro, 8005-139, Portugal и [3]Center of Physics and Engineering of Advanced Materials (CeFEMA), IST, University of Lisbon, Av. Roviscno Pais, Roviscno Pais, Lisbon, 1096-001, Portugal*

Извршена студија дискутује примену Флокеове теорије на 1D Fe–Cu молекулски ланац. Потврђено је да ефекат хибридизације орбитала омогућује испуњење резонантног услова у спектру нижих драјвинг фреквенција ове структуре, што карактерише њену потенцијалну примену у енергетски ефикасним уређајима. Даље, ово је први пут да је Флокеов модел електронског трења (базиран на разматрању утицаја Флокеовог драјва на трансфер електрона) у присуству интеракције светлости и материје (LMI), био примењен на 1D Fe–Cu молекулски ланац. Разматрано је понашање електронске струје, а присуство ограничавајуће фреквенције, која максимизира електронску струју, је потврђено. У оквиру ове студије, постављени су одговарајући модели, који дискутују два начина помоћу којих се може појачати електрична струја под утицајем драјва у јаком LMI режиму: путем ефекта орбиталне хибридизације и путем фотонски потпомогнутих процеса. Добијени резултати би могли унапредити практичну примену материјала који садрже Fe–Cu молекулске ланце у електрохемији.

(Примљено 22. августа2025, ревидирано 5. фебруара, прихваћено 18. марта 2026)

## REFERENCES

1. C. Tang, M. Shiri, H. Zhang, R. T. Ayinla, K. Wang, *Nanomaterials* **12** (2022) 698 (https://doi.org/10.3390/nano12040698)
2. B. Dong, H. L. Cui, X. L. Lei, *Phys. Rev., B* **69** (2004) 205315 (https://doi.org/10.1103/PhysRevB.69.205315)
3. B. D. Fainberg, *Phys. Rev., B* **88** (2013) 245435 (https://doi.org/10.1103/PhysRevB.88.245435)
4. G. Platero, R. Aguado, *Phys. Rep.* **395** (2004) 1 (https://doi.org/10.1016/j.physrep.2004.01.004)
5. G. Floquet, *Ann. Sci. Éc. Norm. Supér.* **12** (1883) 47 (https://doi.org/10.24033/asens.220)
6. Y. Wang, W. Dou, *ACS Phys. Chem. Au* **4** (2023) 160 (https://doi.org/10.1021/acsphyschemau.3c00049)
7. Z. Zhou, H. T., Chen, A. Nitzan, J. E. Subotnik, *Chem. Theory Comput.* **16** (2020) 821 (http://doi.org/10.1021/acs.jctc.9b00950)
8. H. Carias, D. N. Beratan, S. S. Skourtis, *J. Phys. Chem., B* **115** (2011) 5510 (https://doi.org/10.1021/jp111097a)
9. V. Mosallanejad, Y. Wang, J. Chen, W. Dou, *Wiley Interdiscip. Rev. Comput. Mol. Sci.* **15** (2025) e70032 (https://doi.org/10.1002/wcms.70032)
10. M Hromadová, F. Vavrek, *Curr. Opin. Electrochem.* **19** (2020) 63 (https://doi.org/10.1016/j.coelec.2019.10.008)
11. J. Song, E. Khoo, E., M. Z. Bazant, *Phys. Rev., E* **100** (2019) 042204 (https://doi.org/10.1103/PhysRevE.100.042204)

12. Y. Han, C. Nickle, M. S. Maglione, S. K. Karuppannan, J. Casado-Montenegro, D. C. Qi, X. Chen, A. Tadich, B. Cowie, M. Mas-Torrent, C. Rovira, J. Cornil, J. Veciana, E. del Barco, C. A. Nijhuis, *Adv. Sci.* **8** (2021) 2100055 (http://doi.org/10.1002/advs.202100055)
13. E. Leary, B. Limburg, A. Alanazy, S. Sangtarash, I. Grace, K. Swada, L. J. Esdaile, M. Noori, M. T. González, G. Rubio-Bollinger, H. Sadeghi, A. Hodgson, N, Agraït, S. J. Higgins, C. J. Lambert, H. L. Anderson, R. J. Nichols, *J. Am. Chem. Soc.* **140** (2018) 12877 (http://doi.org/10.1021/jacs.8b06338)
14. J. Chen, W. Liu, V. Mosallanejad, W. Dou, *J. Phys. Chem., C* **128** (2024) 11219 (http://doi.org/10.1021/acs.jpcc.4c00969)
15. X. Wei, S. Wei, S. Cao, Y. Hu, S. Zhou, S. Liu, Z. Wang, X. Lu, *Appl. Surf. Sci.* **564** (2021) 150423 (http://doi.org/10.1016/j.apsusc.2021.150423)
16. F. Schwarz, G. Kastlunger, F. Lissel, H. Riel, K. Venkatesan, H. Berke, R. Stadler E. Lörtscher, *Nano Lett.* **14** (2014) 5932 (http://doi.org/10.1021/nl5029045)
17. M. Farsad, M. Elahifard, R. Behjatmanesh-Ardakani, *Theor. Chem. Acc.* **137** (2018) 142 (https://doi.org/10.1007/s00214-018-2346-5)
18. B. J. Lee, B. D. Wirth, J. H. Shim, J. Kwon, S. C. Kwon, J. H. Hong, *Phys. Rev., B* **71** (2005) 184205 (https://doi.org/10.1103/PhysRevB.71.184205)
19. A. I. Fadeeva, V. A. Gorbunov, P. V. Stishenko, A. V. Myshlyavtsev, *J. Phys. Chem. C* **123** (2019) 17265-17272 (https://doi.org/10.1021/acs.jpcc.9b02834)
20. C. Domain, C. S. Becquart, *Phys. Rev., B* **65** (2001) 024103 (https://doi.org/10.1103/PhysRevB.65.024103)
21. *MATLAB version: 9.13.0 (R2022b)*, The MathWorks Inc., Natick, MA, 2022 (https://www.mathworks.com) (accessed 20.06.2025)
22. M. Schönberg, *Nuovo Cim.* **10** (1953), 697 (http://doi.org/10.1007/BF02773031); F. Schwarz, G. Kastlunger, F. Lissel, H. Riel, K. Venkatesan, H. Berke, R. Stadler, E. Lörtscher, *Nano Lett.* **14** (2014) 5932 (http://doi.org/10.1021/nl5029045)
23. J. C. Slater, G. F. Koster, *Phys. Rev.* **94** (1954) 1498 (http://doi.org/10.1103/PhysRevB.94.1498)
24. K. Nakamura, R. Arita, H. Ikeda, *Phys. Rev., B* **83** (2011) 144512 (http://doi.org/10.1103/PhysRevB.83.144512)
25. A.-P. Jauho, N. S. Wingreen, Y. Meir, *Phys. Rev., B* **50** (1994) 5528 (http://doi.org/10.1103/PhysRevB.50.5528)
26. M. Galperin, M. A. Ratner, A. Nitzan, *J. Phys.: Condens. Matter* **19** (2007) 103201 (http://doi.org/10.1088/0953-8984/19/103201)
27. H. Park, J. Park, A. K. L. Lim, E. H. Anderson, A. P. Alivisatos, P. L. McEuen, *Nature* **407** (2000) 57 (http://doi.org/10.1038/35024031)
28. J. Chen, W. Liu, V. Mosallanejad, W. Dou, J. *Phys. Chem., C* **128** (2024) 11219 (http://doi.org/10.1021/acs.jpcc.4c00969)
29. A. P. Sutton, M. W. Finnis, D. G. Pettifor, Y. Ohta, *J. Phys., C* **21** (1988) 35 (http://doi.org/10.1088/0022-3719/21/1/007)
30. C. X. Zhang, M. A. Zubkov, *Phys. Rev., D* **100** (2019) 116021 (http://doi.org/10.1103/PhysRevD.100.116021)
31. M. Holthaus, *J. Phys., B* **49** (2015) 013001 (http://doi.org/10.1088/0953-4075/49/1/013001)
32. D. Zhang, Y. Zeng, Y. Tian, R. Li, *Phot. Insights* **2** (2023) R07 (http://doi.org/10.3788/PI.2023.R07)

33. K. Blum, H. Kleinpoppen, *Phys. Rep.* **52** (1979) 203 (http://doi.org/10.1016/0370-1573(79)90031-0)
34. X. Meng, X. Jing, J. Cheng, H. Tang, X. Chen, X. Zhou, L. Li, *ACS Appl. Nano Mater.* **7** (2024) 8175 (http://doi.org/10.1021/acsanm.4c00709)
35. J. Xie, L. Wang, J. S. Anderson, *Chem. Sci.* **11** (2020) 8350 (https://doi.org/10.1039/d0sc03429k)
36. H. Xiao, G. L. Wu, S. Tan, X. Tan, Q. Yang, *Chem. Asian J* **19** (2024) e202301036 (http://doi.org/10.1002/asia.202301036)
37. J. Liu, K. Luo, H. Chang, B. Sun, Z. Wu, *Nanomaterials* **11** (2021) 2713 (http://doi.org/10.3390/nano11102713)
38. J. M. Raulot, C. Domain, J. F. Guillemoles, *Phys Rev., B* **71** (2005) 035203 (http://doi.org/10.1103/PhysRevB.71.035203)
39. M. Acquarone, P. Monachesi, *Phys Rev., B* **38** (1988) 2555 (http://doi.org/10.1103/PhysRevB.38.2555)
40. M. Moskalets, M. Büttiker, *Phys Rev., B* **78** (2008) 035301 (http://doi.org/10.1103/PhysRevB.78.035301)
41. Violeta10203 (2026). Floquet_1D_Fe_Cu_system (Version v3.0) [Matlab code], Zenodo, https://doi.org/10.5281/zenodo.19096574.